J. Fluid Mech. (1985), *vol.* 152, *pp.* 125–143
Printed in Great Britain

A perspective view of the plane mixing layer

By JAVIER JIMENEZ,
IBM Scientific Centre, Paseo Castellana 4, 28046-Madrid, Spain

MARTA COGOLLOS
School of Aeronautics, Universidad Politécnica Madrid, 28040-Madrid, Spain

AND LUIS P. BERNAL†
California Institute of Technology, Pasadena, CA 91125

A three-dimensional model of the plane mixing layer is constructed by applying digital image processing to laser fluorescence motion pictures of the layer, and displayed using computer graphic techniques. A system of streamwise counterrotating vortices is shown to exist on top of the classical spanwise eddies, and its influence in mixing is discussed briefly. Some quantitative information on their strength is also given.

1. Introduction

Some evidence has appeared lately implying that the nominally plane turbulent mixing layer contains secondary structures involving the deformation of the primary large-scale eddies along their span (Konrad 1976; Browand & Troutt 1980; Roshko 1980; Jimenez 1983). These structures have been interpreted in some cases as being produced by an array of longitudinal (streamwise) vortices lying approximately on the braids connecting consecutive primary (spanwise) eddies (see figure 1). Such an arrangement had been predicted theoretically on the grounds that any streamwise vorticity injected accidentally into the braids would be stretched by the straining field produced by the primary eddies into long longitudinal vortices (Corcos 1979). Since there is no obvious mechanism to introduce net streamwise vorticity in the flow, the longitudinal vortices are expected to alternate in sign, in such a way that their total net vorticity is zero. Some measurements of the strength of these proposed longitudinal vortices were presented in Jimenez (1983), where their circulation was shown to be of the same order as that contained in each wavelength of the primary Kelvin–Helmholtz spanwise instability. This suggests that the longitudinal structures form early in the evolution of the layer as a result of the deformation of the two-dimensional eddies by a secondary instability.

The linear phase of such instabilities was studied theoretically by Pierrehumbert & Widnall (1982) and takes the form of a wave-like deformation along the span of the two-dimensional vortices. Such a wave-like structure is strongly implied by pictures of the transition region published by Breidenthal (1981). The idea is that, in the nonlinear stage of their evolution, those waves are stretched by the Corcos (1979) mechanism to give the elongated structures observed later in the flow. While all the above evidence makes the existence of longitudinal vortices highly plausible, no direct evidence of their existence had been presented until recently. The motion

† Present address, Dept Aerospace Engineering, University of Michigan, Ann Arbor, Mich., 48109.

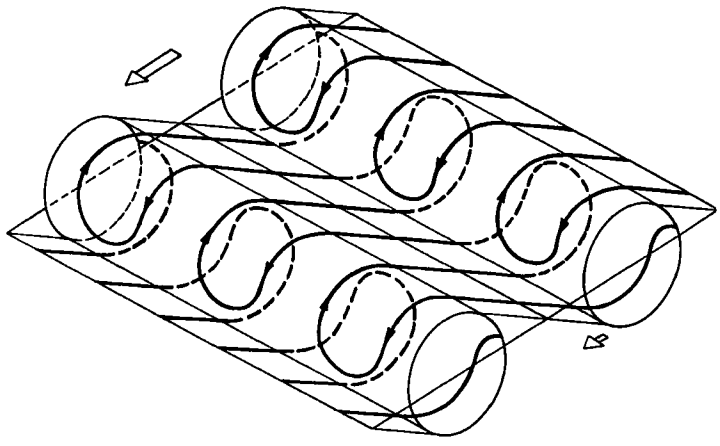

FIGURE 1. Model for streamwise vorticity distribution. After Bernal (1981*b*).

pictures published in Roshko (1980) and Bernal (1981*b*) offer a direct visualization of spanwise sections of the concentration field and clearly show longitudinal structures compatible with the vortex-array model. We analyse here those pictures using image processing and computer graphic techniques with the purpose of reconstructing the three-dimensional topology of the flow and of determining the influence of the longitudinal structure on mixing. Some quantitative analysis of vortex strength is also given.

2. Experiment and data processing

The experimental arrangement and the original motion pictures are described in Bernal (1981*b*). The apparatus itself is the one used in Breidenthal (1981). A mixing layer is established between two water streams in a blow-down tunnel with a 7×11 cm cross-section. One of the streams – the low-speed one – contains a dye that fluoresces when illuminated with a sheet of laser light of appropriate wavelength, arranged perpendicularly to the stream direction. Since the dye is transparent to the fluorescent radiation, the illuminated sections can be observed through the body of the dyed stream (Dimotakis, Miake-Lye & Papantoniu 1983). For our analysis we have used motion pictures of one such section, taken at a fixed downstream location, as it evolves in time. A frame from one of the films is shown in figure 2(*a*); the flow comes toward the observer and the dye is contained in the light-coloured region on top. That frame corresponds to a section through a braid separating two primary eddies, and the 'curly' structures visible in the interface are the ones presumably due to the longitudinal vortices.

Another section, taken at a higher Reynolds number, is shown in figure 2(*b*), which is predictably more complex but still shows structures of the same type as the ones at lower Reynolds number. All the images were taken at a distance of 17 cm from the splitter plate, and the Reynolds number was controlled by changing the free-stream velocities. The momentum thickness of the boundary layer at the high-speed side of the splitter plate was not measured directly in this experiment, but it can be inferred from the values given by Breidenthal (1981) for the same apparatus. A summary of flow parameters for the two films used in this paper is given in table 1. The downstream position of the illuminated section, expressed as a multiple

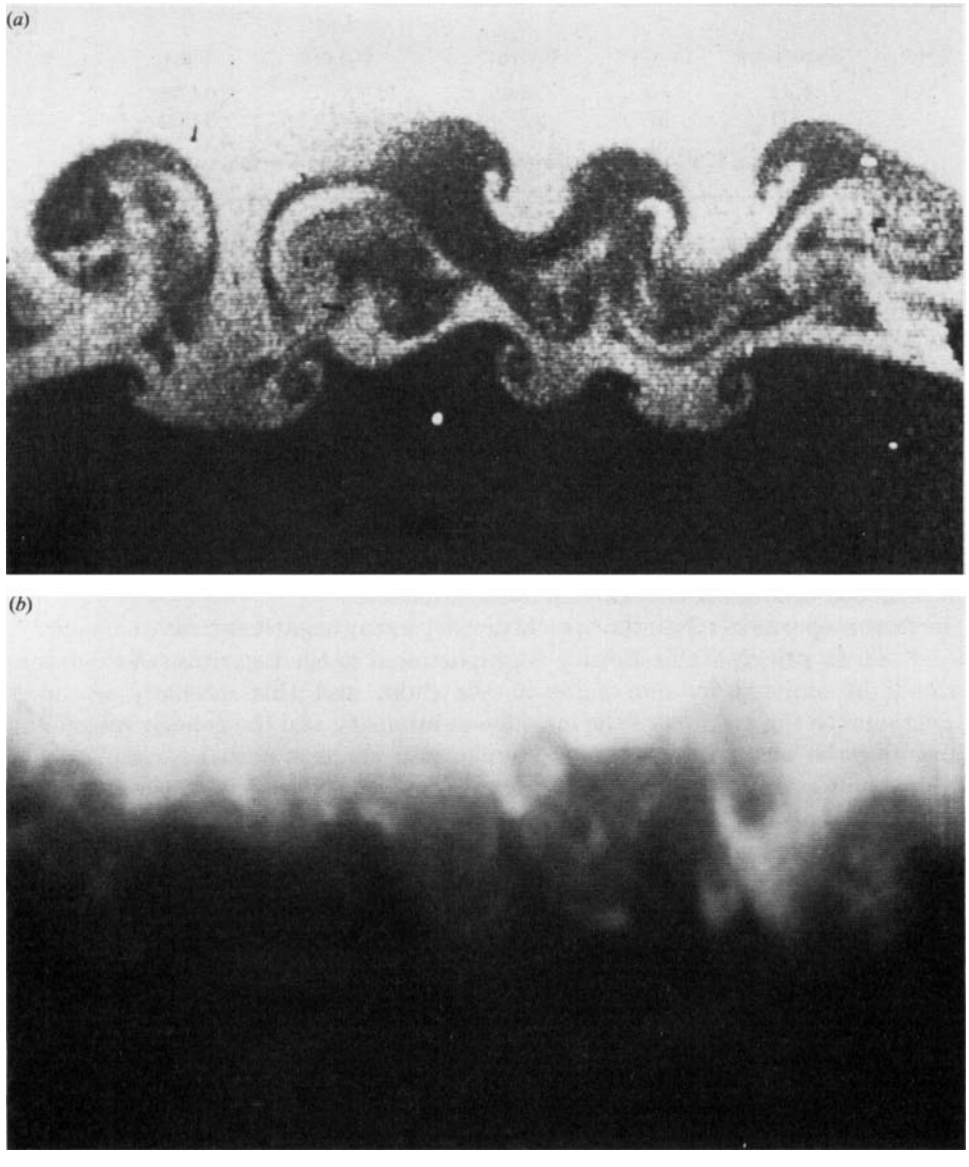

FIGURE 2. Two frames from the films analysed in this paper: (*a*) film A; (*b*) film B. Dye is on the low-speed stream on the top of the pictures.

of the initial boundary-layer thickness θ, is seen to be about 300 for the low Reynolds number film and 600 for the high Reynolds number one. According to the values given for the three-dimensional transition by Breidenthal (1981) and Jimenez (1983), the first film would correspond to the growth region of the three-dimensional instability, while the second one would already be in its well-developed region.

From these two films we have extracted three sequences, two corresponding to the low and one to the high Reynolds number case. Each sequence is formed by approximately 200 consecutive frames. Each frame was digitized and treated as the transverse section of a three-dimensional solid. The third dimension, time, was converted to space (x) by using a fixed convection velocity equal to the average

Film	Sequences	U_1 (cm/s)	U_2 (cm/s)	$(U_1-U_2)x/\nu$	θ (cm)	x/θ
A	I, II	15	6.4	14600	0.052	330
B	III	52	20	54400	0.028	613

TABLE 1. Flow characteristics of the films used for this paper

between the two free-stream speeds. The adequacy of this hypothesis will be discussed later. Digitization converts each frame into a large numerical matrix in which each value represents the optical transmissivity at one point of the photographic negative. When all the consecutive frames are stacked together, they form a three-dimensional array which is a digital model of fluorescence intensity in the mixing layer. Any section of this model, not just the original transverse ones, can now be displayed on a computer terminal. Figure 3 shows longitudinal sections of the three sequences treated in this paper. These sections correspond to the classical two-dimensional pictures of, for example, Brown & Roshko (1974) but, since now the coordinates are y, t instead of y, x, the eddies are all at the same stage of their development and do not appear to grow. Sequences I and III contain several 'normal' eddies; sequence II was chosen because it contains an amalgamation.

The next step was to relate the optical density in the negatives to dye concentration in the fluid. In principle this density is proportional to the logarithm of the intensity of the light emitted by one point in the fluid, and this intensity is, in turn, proportional to the product of the laser beam intensity and the concentration of dye. In practice the beam intensity is unknown and changes across each picture and, although calibration is possible, it was not done when the present films were obtained.

The main reason for the variation of beam intensity from point to point is light absorption by the dye. This is quite noticeable in figure 2(*a*) as a gradual darkening of the frame as one moves from the top, where the beam enters the test section, to the bottom of the dyed region. By examining individual vertical profiles for the frames in sequence I, it can be estimated that this darkening amounts to almost 40 % of the difference between the two streams. In principle, that effect can be corrected by noting that the beam intensity decreases at a rate which is proportional to the local dye concentration. After some manipulation, the concentration C can be related to the emitted intensity E by

$$C = \frac{E}{B(1-A\int E\,\mathrm{d}y)},$$

where B is the intensity of the beam at a reference point, A is the constant absorption coefficient, and the integral extends along the beam from the reference point to the point being measured. Since many variables, including the film response, are unknown in the absence of calibration, this formula is difficult to apply. A rough approximation was made by assuming that the optical transmittance in the film was linearly related to emitted light intensity. The reference intensity B and the coefficient A were then estimated by using two points in the free stream, throughout which the concentration was assumed to be constant and known. The correction was applied to film sequence I, and was partially successful in that the grey level in the dyed stream was relatively uniform after the correction. This can be seen by comparing figure 3(*a*), which is corrected, to 3(*b*), to which no correction has been applied. There is, however, no guarantee that the resulting images are accurate enough to use in more than a qualitative analysis of the concentration distribution.

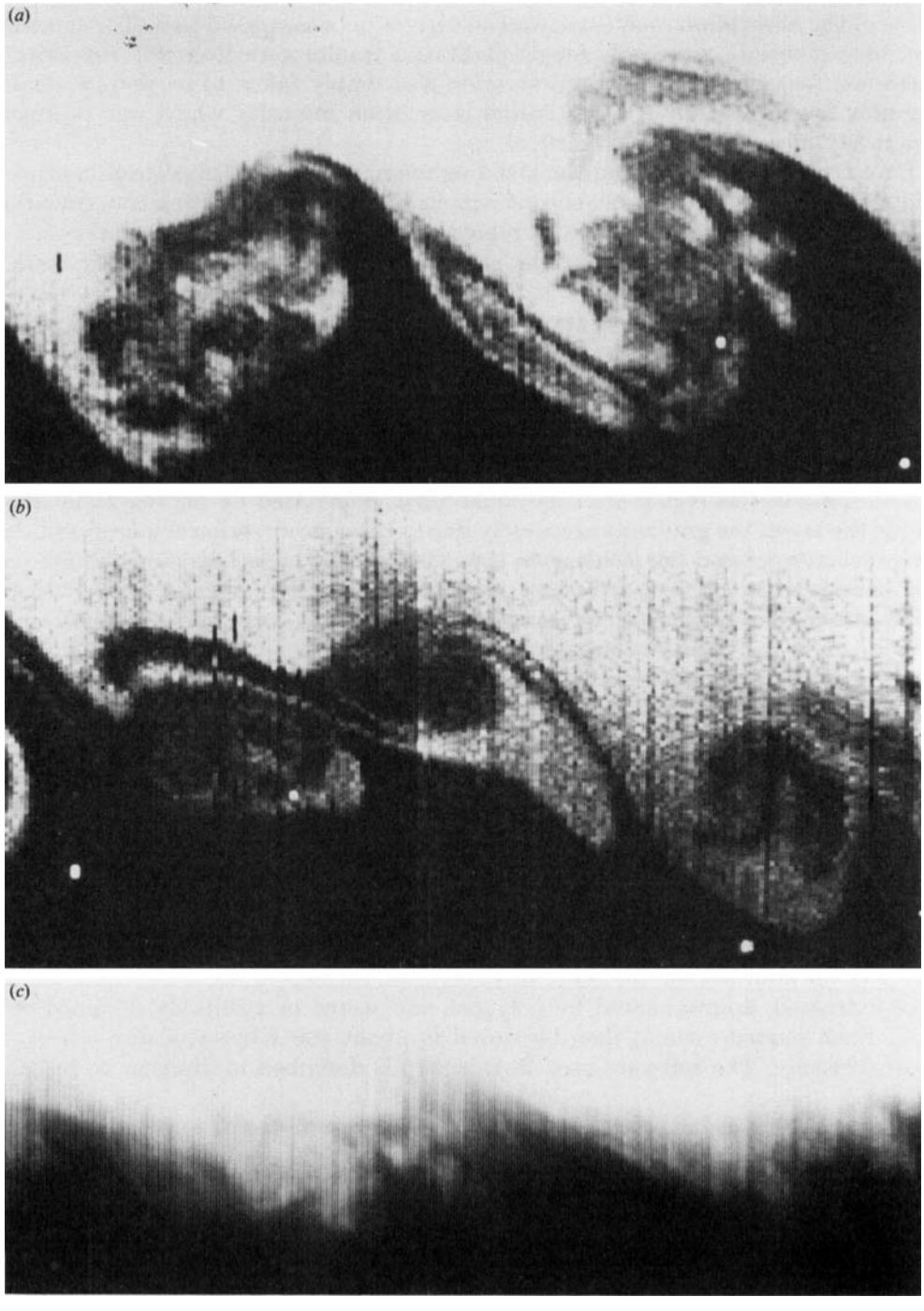

FIGURE 3. Streamwise sections of the three sequences used in the reconstructions.

Sequence III (the high-speed case) did not have enough free stream to estimate the value of the absorption coefficient, and no correction was applied to it. The same was true of sequence II, since only rough qualitative results were desired in this case. In these last two sequences the concentration was simply taken to be proportional to the grey level, normalized by an initial laser beam intensity which was estimated separately for each incoming (vertical) ray.

Each frame was filtered using a local sliding average over a 5×5 pixel neighbourhood, and classified into three homogeneous regions based on the resulting concentration. These three regions are intended to represent each of the two free streams plus an intermediate 'mixed' layer, but the choice of the thresholds separating them is somewhat arbitrary. In general it is quite easy to define thresholds giving the approximate 'outer' limits of the mixing layer, particularly in the low Reynolds number case, in which there is a visually sharp interface between mixed and unmixed fluid. However because of the beam absorption problem, those thresholds cannot be defined simply in terms of percentages of the grey levels in the free streams.

A good empirical criterion is the vertical grey level gradient. Outside the layer, this gradient is only due to beam absorption and is fairly mild. As a consequence, the isolevel lines in this region are very convoluted, dominated by photographic noise. Inside the layer, the gradients are mostly due to the concentration changes, and they are much steeper and the isolines are smoother. In the high Reynolds number case the distinction is not so clear but an outer limit can still be defined. Inner views of the layer can then be obtained by using tighter thresholds, spanning only some central percentage of the total concentration range.

The classified frames had to be smoothed further to eliminate the 'salt and pepper' noise. This was done by using a three-dimensional majority voting scheme. Each element in the three-dimensional numerical array was considered as the centre of a $3 \times 3 \times 3$ cube; the number of elements in the cube belonging to each class was counted, and the centre pixel was assigned to the class of the majority. The result of classification and filtering on figure 2(*a*) is shown in figure 4.

The amount of storage needed for each sequence, when stored in this fashion, was relatively large. Each numerical array is approximately $200 \times 350 \times 450$ and, therefore, contains over 30 million elements. As a result, the arrays had to be kept in magnetic tape and could not be accessed fast enough for interactive display. To compact the information, the contours of the class corresponding to the 'mixed' fluid were extracted, approximated by polygons and stored in a suitably designed data base. Each sequence could then be stored in about 400 Kbytes of disc space and accessed easily. The software used in this step is described in Jimenez & Navalon (1982).

The three film sequences were digitized at different moments and using different techniques. The pixel size was, in all cases, close to 20 μm on the film negative, corresponding to about 0.2 mm on the flow. Sequence I was digitized using the Perkin Elmer 1010MP flat-bed microdensitometer at the IBM Madrid Scientific Centre. Sequences II and III were scanned using a Vidicon camera attached to a De Anza image-processing system at the Jet Propulsion Laboratory. The grey scale used in the first two sequences was linear in the amount of transmitted light while, for the third, a logarithmic scale was used to improve the contrast slightly. The subsequent processing was done, in all cases, using the facilities at the IBM Centre, consisting of a mainframe computer (IBM 370/158MP) and peripherals.

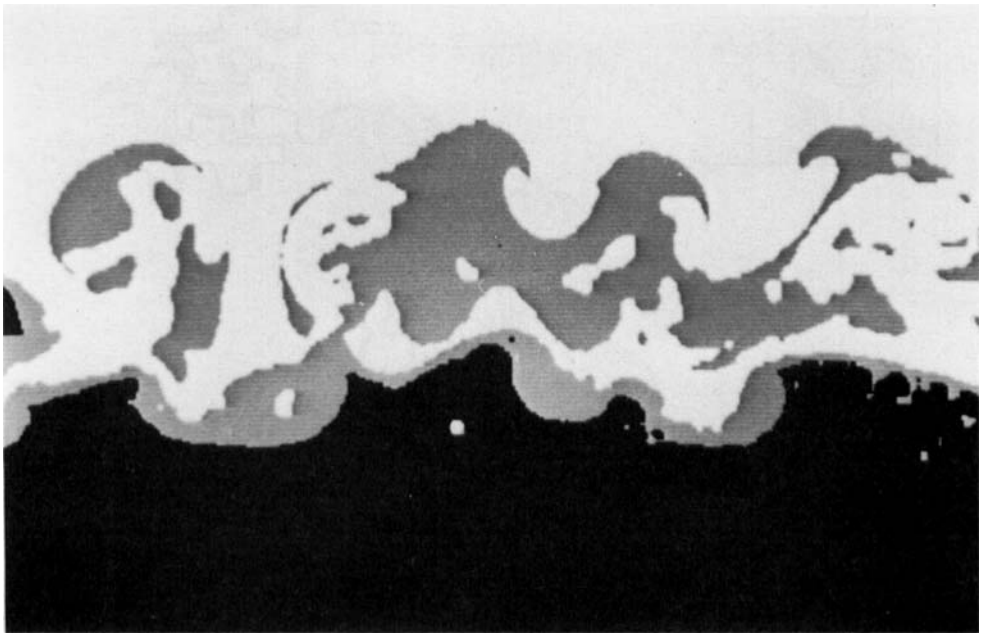

FIGURE 4. Segmented version of the figure 2(*a*), after classification and filtering.

3. Three-dimensional reconstruction

The polygons stored in the data bases generated above represent sections of a three-dimensional model of the mixing layer but, to visualize that model, some form of graphic representation was needed. Several methods are available for the display of complex three-dimensional objects on a computer terminal, many of which are surveyed in the book by Foley & Van Dam (1982). We generated our solid model by constructing, for each section, a short cylinder (actually a prism) based on its polygonal contour and extending in the direction of the flow with a depth equal to the convection distance between frames. These prisms were then stacked together to form a polyhedral body (see figure 5).

The resulting solid was displayed on a black and white computer monitor and photographed directly from the screen. The method used for hidden surface elimination was a slightly modified depth buffer (see Foley & Van Dam 1982, chap. 15). Shading of the surfaces was done assuming that the object was illuminated by a single point source, with a small amount of extra isotropic illumination (Phong 1975). No shadows were computed, but the resulting unnatural aspect of the representations was controlled by keeping the light source close to the observer. Both the orientation of the model and the position of the source could be controlled interactively, as was the clipping of the model by an arbitrary plane. The computer time needed for a complete display was between one and three minutes.

The model for sequence number I, extracted from the low Reynolds number film, is shown in figure 6. The flow runs from the bottom left to the top right corners of the picture and the two large horizontal structures are the classical Brown–Roshko eddies. The mixing layer is seen from its low-speed side, looking downstream, and a remarkably regular array of streamwise structures is seen superimposed on the primary eddies. The high-speed side of the same sequence is shown in figure 7, and

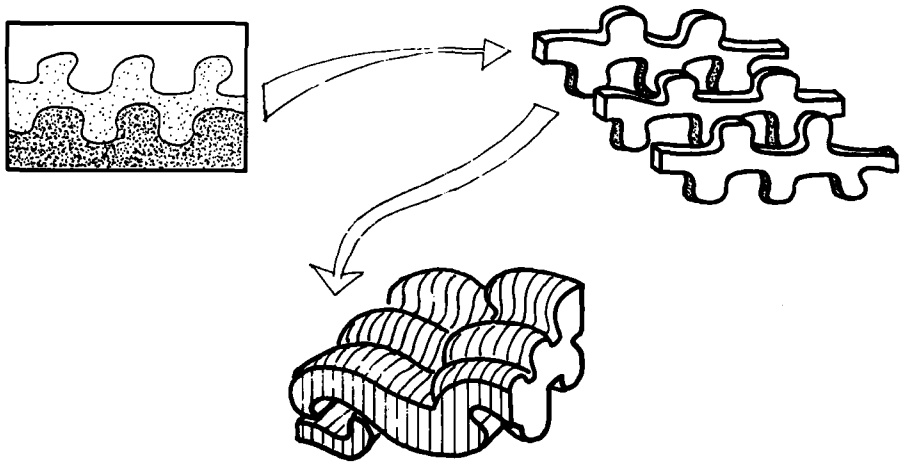

FIGURE 5. Reconstruction of a three-dimensional solid from the transversal sections.

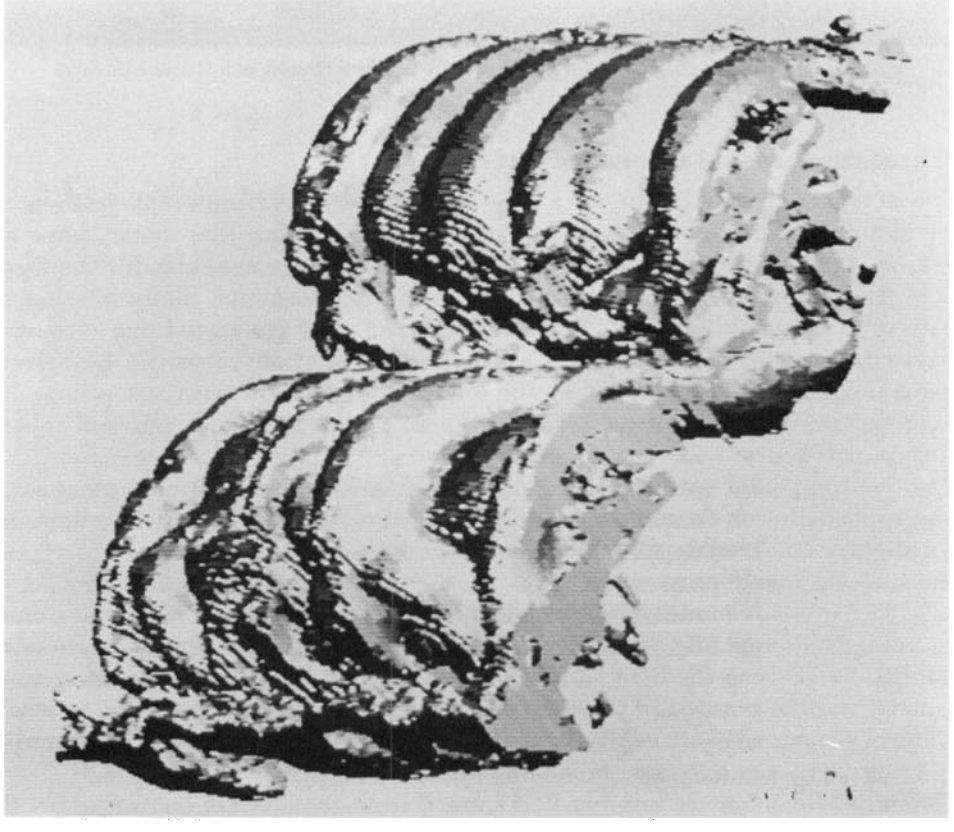

FIGURE 6. The low Reynolds number mixing layer. Sequence I, seen from the low-speed side, looking downstream. Flow is from bottom left to top right. Concentration thresholds were chosen to span 40% of concentration distribution.

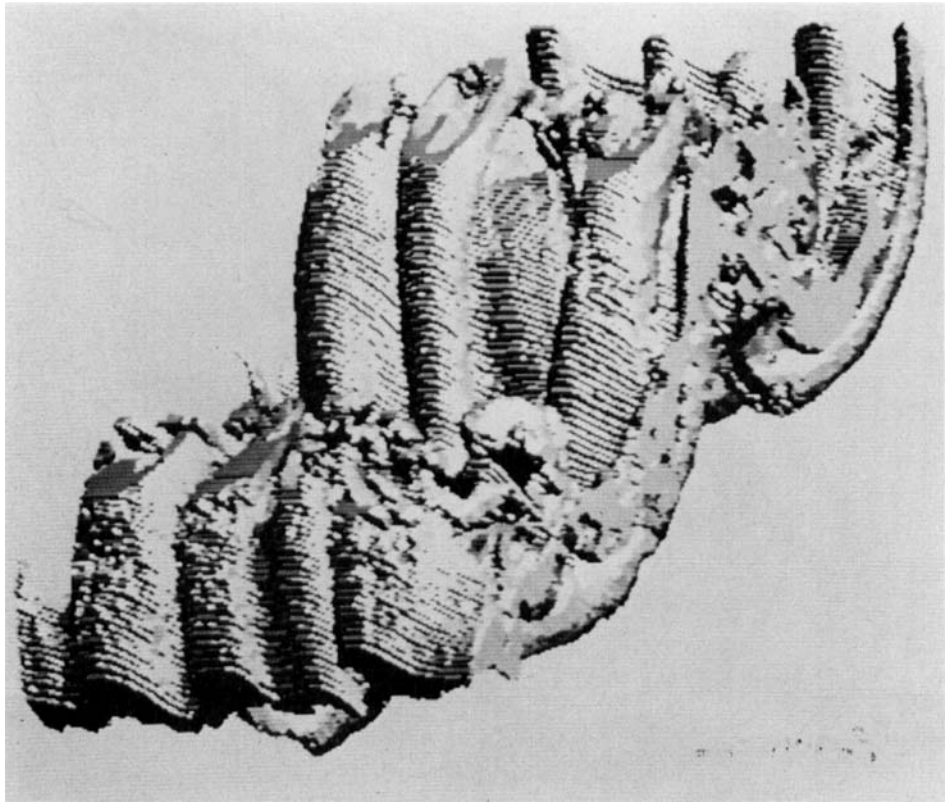

FIGURE 7. As figure 6, seen from high-speed side. A section by horizontal plane on the top shows the interior structure of the streamers.

contains the same streamwise structure. In this figure the layer has been cut by a horizontal (z,t) plane, showing that the interior of at least some of the streamers contains two hollow (unmixed) tubes strongly suggestive of a vortex pair.

The thresholds used to isolate the mixed fluid for these two figures are relatively 'narrow' ones, adjusted to span approximately the central 40% of the concentration distribution. The equivalent of figure 6, but with ' wide' thresholds containing most of the mixed fluid, is shown in figure 8; the qualitative structure of the concentration field is not changed by this choice.

In both figures 6 and 8 it is somewhat surprising that a fairly large amount of mixed fluid is apparently present in the thick streamers of the braid region, where mixing would normally not be expected. Figure 7 shows that this is not the case. Particularly in the eddy at the rear of the picture, the braid is seen to be a thin shell, containing little mixed fluid, but deformed by the secondary flow. The convex parts of these corrugations are what appears to form the thick, but actually hollow, streamers in the braids. Interestingly, the densest concentration of mixed fluid is not found at the core of the large eddies; figure 6 shows quite a lot of empty (unmixed) space in that region. That is confirmed by figures 9 and 13, which are side views of the film sequences I and II, both of the low Reynolds number flow. These figures correspond to the classical two-dimensional view of the layer and they allow us to look along the axes of the spanwise eddies. In both cases most of the mixing seems to happen above and

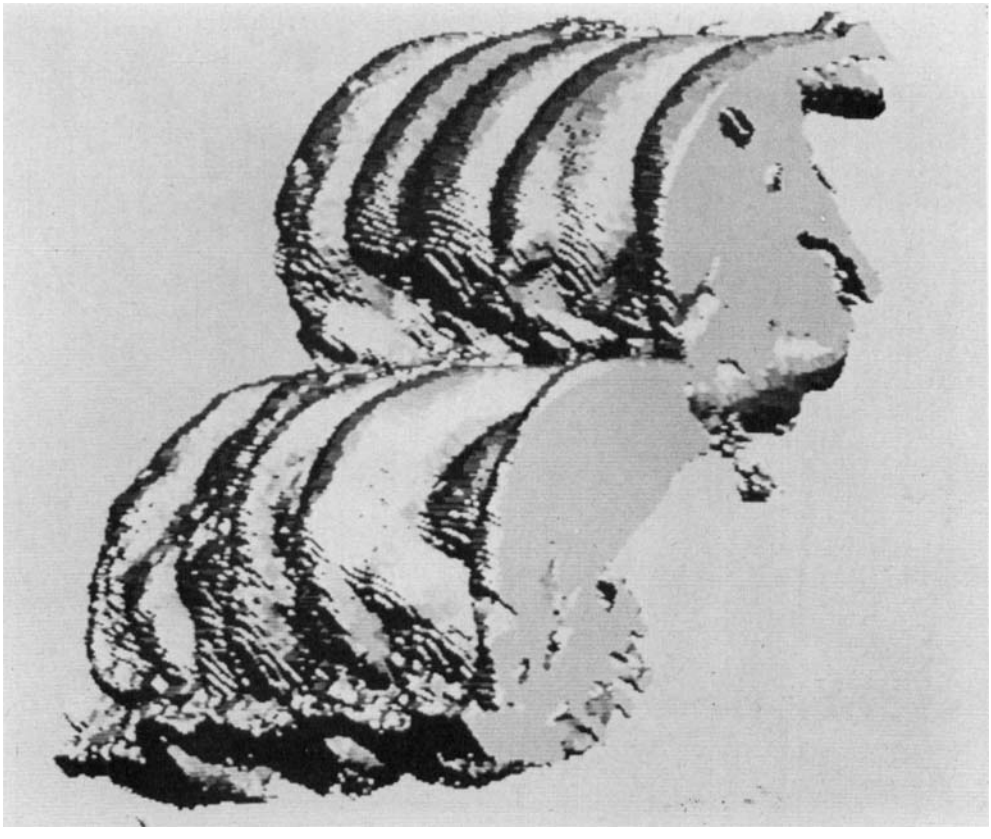

FIGURE 8. As figure 6, but thresholds were adjusted to span most of the mixed fluid.

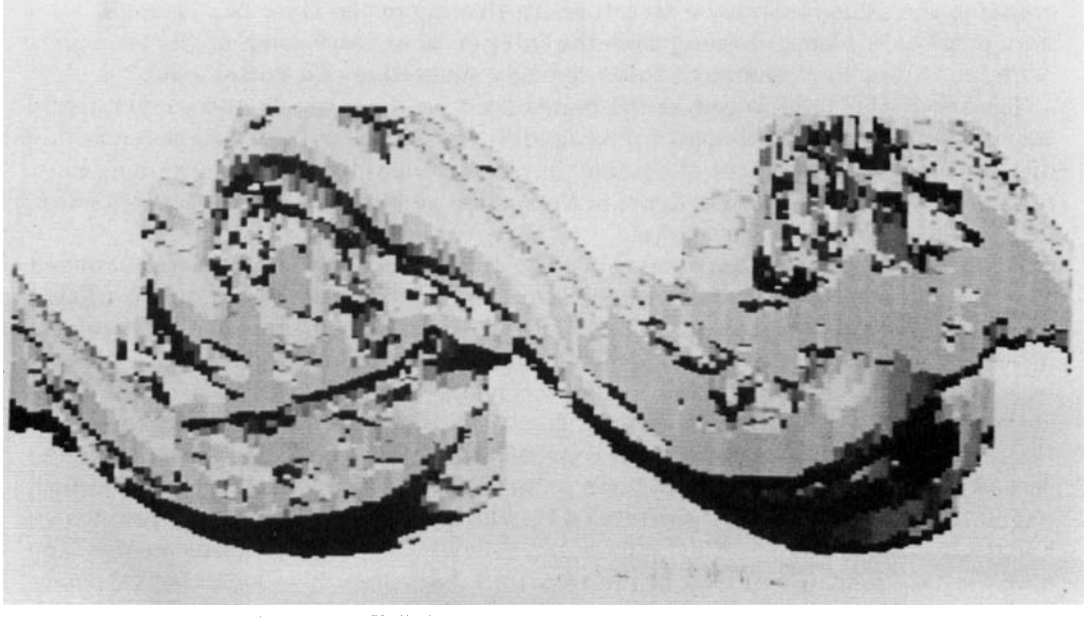

FIGURE 9. Side view of sequence in figures 6–7; inner thresholds.

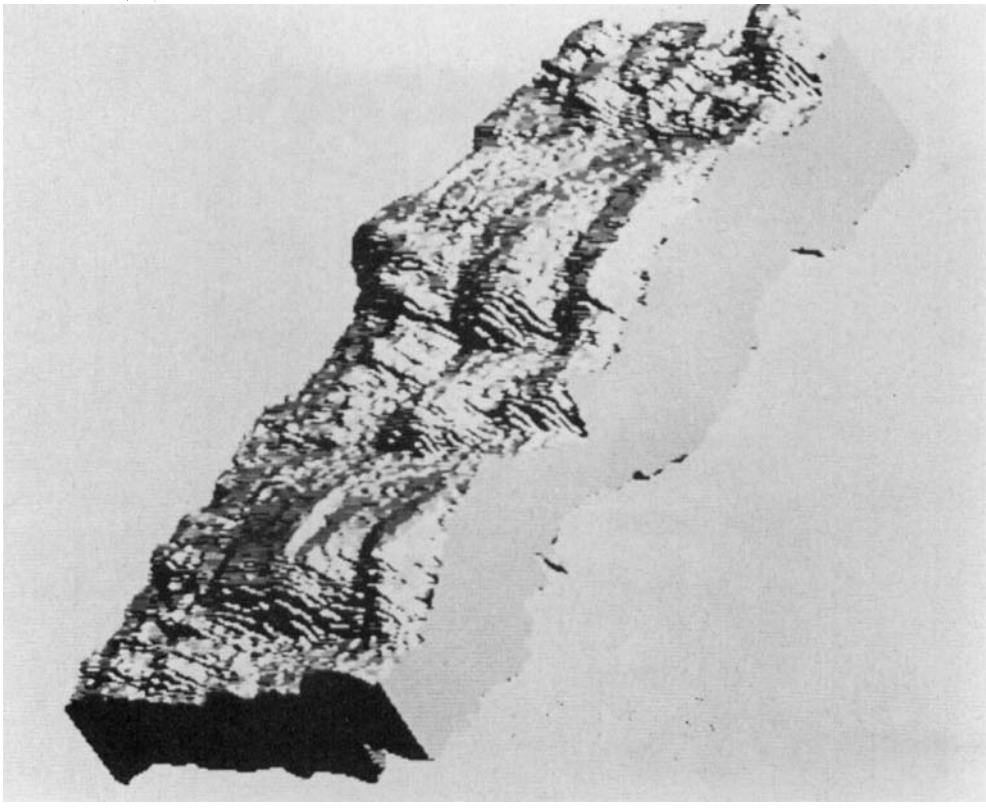

FIGURE 10. Sequence III, high Reynolds number, seen from the high-speed side, looking upstream.

below the eddy, and this impression is generally supported by other sections, not shown here, of the low Reynolds number film.

A picture of the high Reynolds number sequence is shown in figure 10. Figure 11 shows the same sequence with the mixed fluid defined with tighter thresholds. In both views, the streamwise structure is noticeable and quite organized, especially in the 'inner' version, but in none of them is there any pocket of unmixed fluid inside the layer, showing that in this case mixing is more uniformly distributed.

A simple explanation for these mixing distributions is possible. At very low Reynolds numbers the vorticity field is two-dimensional, concentrated in the spanwise cores, and the mixing is low. During the three-dimensional transition, corresponding to our first film, the streamwise vortices appear in the braids, but the vorticity is still largely two-dimensional both in the cores (spanwise) and in the braids (streamwise). The only real three-dimensionality is in those places in which both systems intersect, above and below the classical cores. It is only there that mixing is enhanced. Further downstream, small-scale turbulence is either produced or convected throughout the layer and mixing is more uniform.

The different aspect of the two layers has another consequence. In the low Reynolds number flow the concentration interface is sharp, and the presence of a three-dimensional configuration of freshly drawn fluid inside the layer strongly implies the existence of active streamwise, and spanwise, vortices. In the high Reynolds number

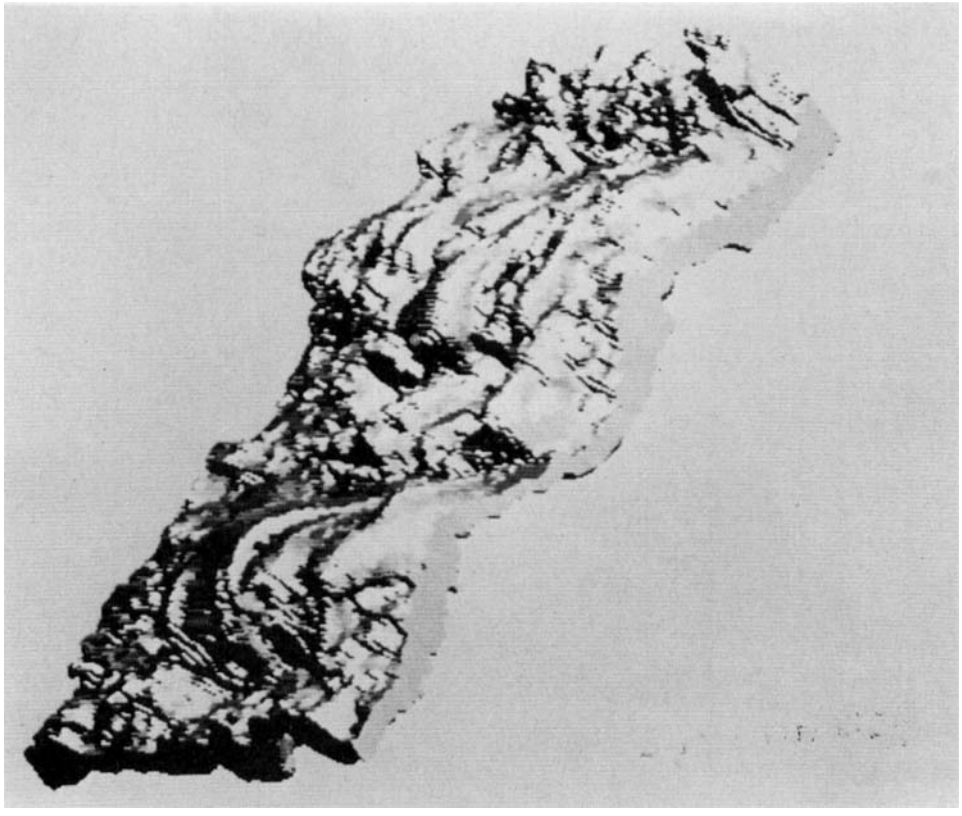

FIGURE 11. As figure 10, but inner (40 %) concentration thresholds.

case there is no direct evidence of freshly drawn fluid inside the layer, either two- or three-dimensional, and it is not possible to deduce much about the present, as opposed to past, vorticity distribution. Jimenez (1983) presents evidence of active, although relatively weaker, longitudinal vorticity in this region.

Figure 12 is a reconstruction of a sequence from the low Reynolds number film containing an amalgamation. On the top part of the figure the layer is seen from its high-speed side and the pairing appears as a long 'hook' extending from below the second eddy into the third. The low-speed side and a lateral view of the same sequence are shown in the bottom part of figure 12 and in figure 13; the pairing is now a single continuous structure embracing the two eddies. The difference between the top and the bottom views is striking but, most probably, is due to a failure of the convection hypothesis. As a pairing occurs, the downstream eddy is carried far into the low-speed stream and is decelerated at the same time as the other eddy is accelerated by the fast stream. As a consequence, and since we are observing the layer at a fixed downstream station, the former eddy stays longer in our field of view and looks elongated, while the latter is accelerated past the observation section and looks shorter. In fact, what we are seeing in figure 12 is not only the same object seen from two different points of view but also, in part, an earlier and later version of the same phenomenon. It is fascinating nevertheless to observe that, in the low-speed paired view, only three longitudinal streamers have survived, compared to twice as many

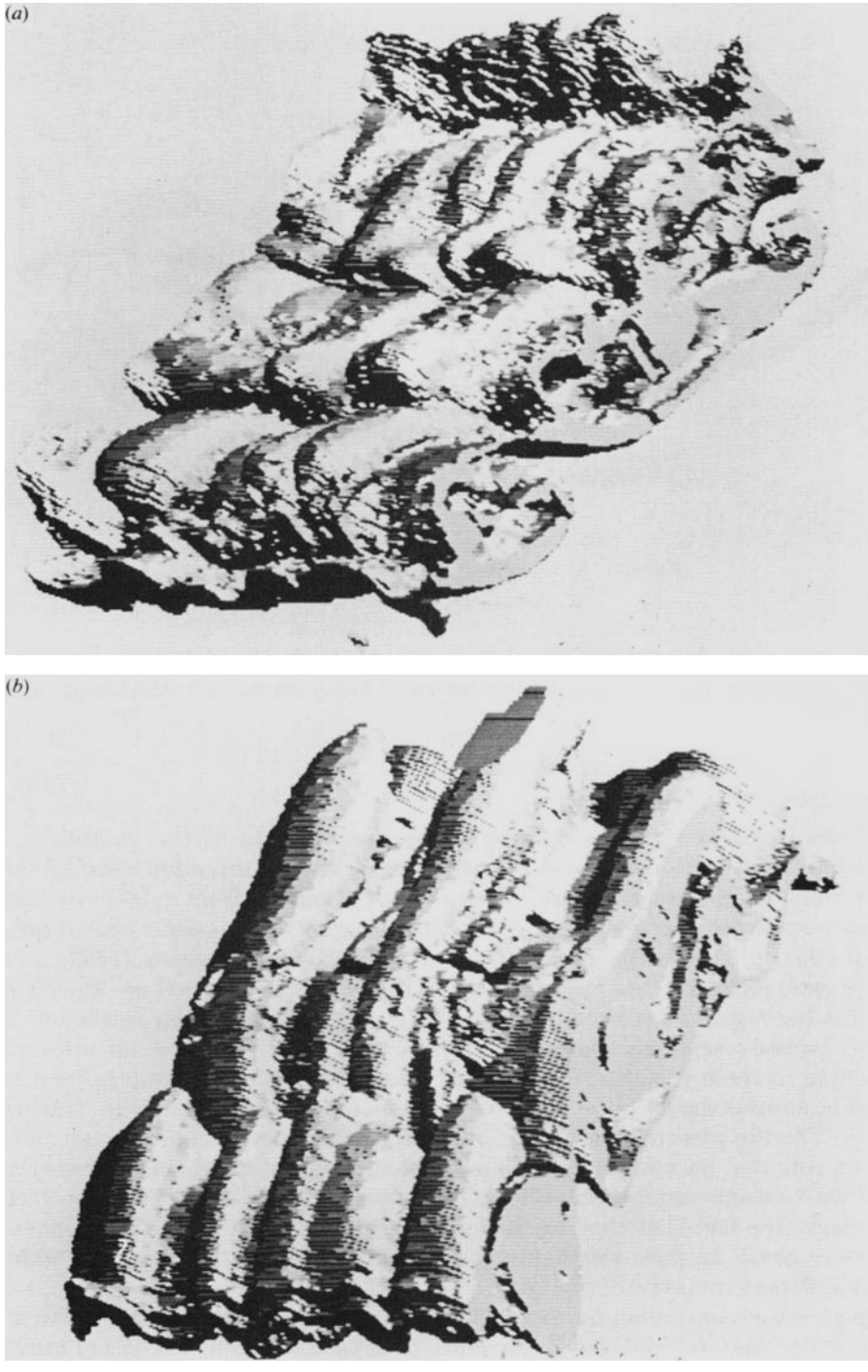

FIGURE 12. Sequence II, low Reynolds number, including a pairing: (*a*) high-speed side, looking upstream; (*b*) low-speed one. Concentration thresholds 50%.

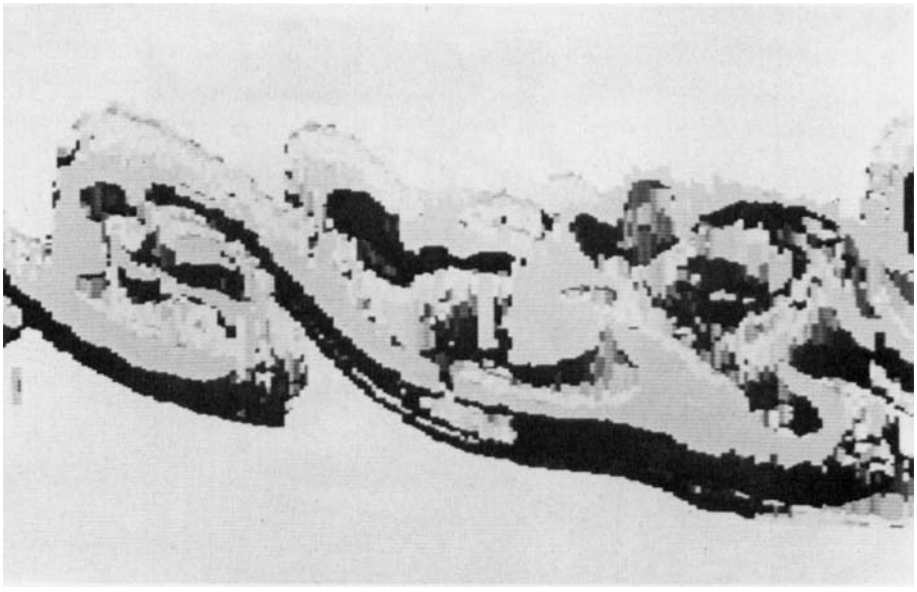

FIGURE 13. Side view of the layer in figure 12.

on the other side. Apparently the flow is able to sense the change in scale of the primary structure and to adapt itself rather quickly so as to maintain geometric similarity.

4. The convection hypothesis

The two different views in figure 12 raise the question of the validity of the convection hypothesis; more precisely, whether the same convection velocity can be used throughout the layer. Figure 14 shows data extracted from a different film; in this case a spanwise averaged view of a mixing layer between gases of similar density (Bernal 1981*a*). This is the same film used by Hernan & Jimenez (1982) and its velocity ratio (0.38) is quite close to those of the two films used before. The outlines of the mixing region have been extracted by a process very similar to the one used for the spanwise sections, and represented in a plotter. There is no attempt at perspective in these pictures. Each section has been displaced upwards by a fixed amount and backwards by a distance corresponding to the average convection velocity. The top picture shows the view from the fast stream, and the bottom one has been reflected on a horizontal plane to show the low-speed side. If everything moved with a single convection velocity the traces of all the eddies would be vertical in the page; the fact that they are not proves that each side of the layer moves at a different speed. In fact, this figure suggests a view of the mixing layer which is slightly different from the normal one.

In the average convection frame an eddy grows and is deformed by the mean shear in such a way that the high-speed part moves forward while the low-speed part lags behind. These two parts follow fairly straight trajectories but the growth is enough to prevent them from splitting apart. In the process, the eddy just upstream, which is usually smaller because it is at an earlier stage of its development, is occasionally engulfed and disappears. The large eddy is not specially perturbed by this process.

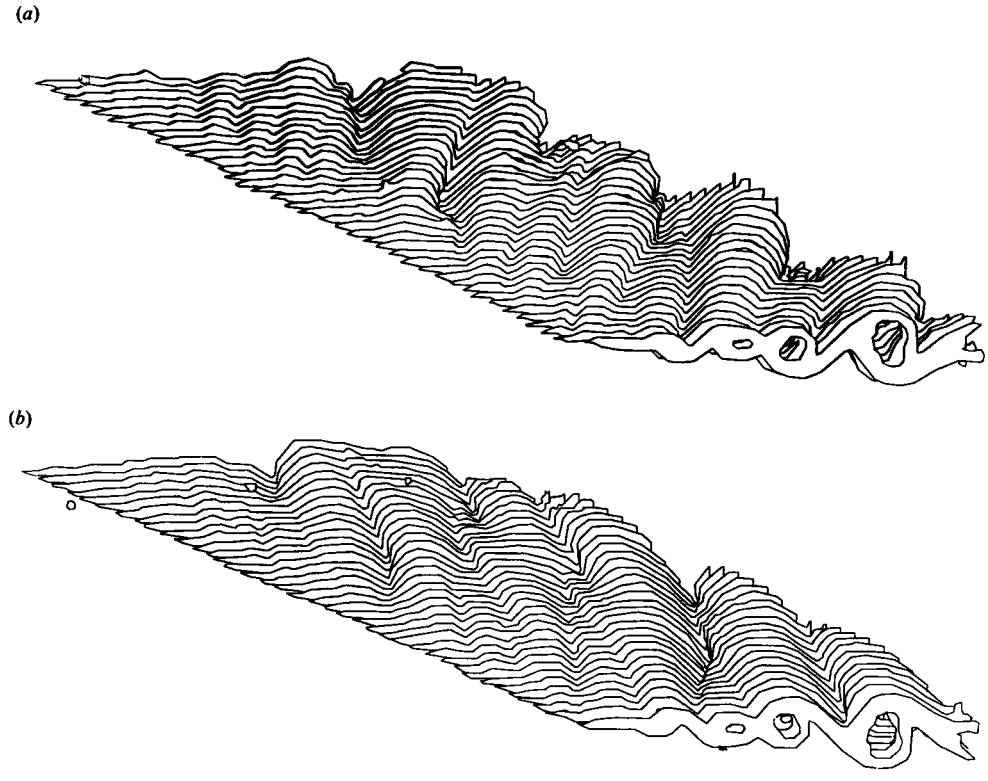

FIGURE 14. Top and bottom view of spatially growing layer showing different convection velocities: (*a*) high speed side; (*b*) low.

Since the smaller eddy is normally the one that is carried into the fast stream, this creates an asymmetry between the two sides of the layer which is evident in figure 14. The high-speed side contains only one set of velocities, which are those of the tops of the large eddies, and which are not changed during pairings; the low-speed side contains the velocities of the lower part of those large eddies plus those of the smaller ones, but these velocities change occasionally when a pairing is involved. This asymmetry is interesting in view of the reports by various investigators of different amounts of entrainment on both sides of the mixing layer (Konrad 1976; Broadwell & Dimotakis private communication).

From figure 14 it is possible to estimate the ratio of the convection velocities on both sides as being close to 1.3, with the deviation from the average velocity approximately equal in both cases. If we interpret the difference between convection velocities as a fixed fraction of the difference between the two free streams, that fraction is approximately 0.35. In a half jet, this would imply convection velocities equal to 0.33 and 0.72 times the mean flow speed, which are close to the ones given by Hussain & Clark (1981). For our velocity ratio the difference is not large enough to invalidate the approximate use of the convection hypothesis in the construction of the models. The only exception is probably during pairings, as shown by figure 12.

5. Estimation of vortex strength

Assuming that the streamwise structures are indeed an array of counterrotating vortices, it is possible to get an estimate of their strength by assuming that the position of the concentration interface has reached a state of equilibrium between the motions induced by the spanwise and the streamwise vorticity fields. Consider figure 15: moving in the average convection frame of reference, the fluid near the mid-point between two large spanwise eddies sits on a stagnation line. In the plane AA' we have the situation shown in the right-hand part of the figure, with the alternating-vortex system sitting on the dividing streamlines of the cat's-eye pattern produced by the spanwise cores. The incoming flow produced by the straining field of the stagnation line tries to keep the concentration interface close to its undisturbed position, while longitudinal vortices tend to displace it in the way shown in the picture.

For a fluid particle equidistant from two longitudinal vortices, the equation of motion is then

$$\frac{\mathrm{d}y}{\mathrm{d}t} = \frac{\gamma}{2b\cosh(\pi y/b)} - \frac{\pi\Gamma}{2\lambda^2}, \tag{1}$$

where the first term of the right-hand side is the velocity induced by the longitudinal system, and the second one is the strain induced by the spanwise vortices. The two effects are at equilibrium at point $y = h$, which satisfies

$$\frac{\pi h}{b}\cosh\left(\frac{\pi h}{b}\right) = S; \quad S = \frac{\gamma}{\Gamma}\left(\frac{\lambda}{b}\right)^2, \tag{2}$$

and it is easy to see that, after a sufficiently long time, the interface will be deformed into a series of alternating up and down structures whose amplitude approaches the one given by (2). Actually, this is only true for infinite time, and it is interesting to estimate the rate of approach.

The timescale of (1) is

$$T = \lambda^2/\Gamma$$

and the behaviour of the solution is controlled by the dimensionless parameter S on the right-hand side of (2), which measures the ratio between the strains induced by the longitudinal and the spanwise vortex systems. It will be seen below that, in our case, this parameter is large (about 20) and, under those conditions, the solution to (1) approaches to within a few percent of the equilibrium point in a time of the order of $T/\log(2S)$, which is small with respect to T.

The related problem of the collapse of the longitudinal vorticity into the compact cores used in our model has been treated numerically by Lin & Corcos (1984). They study the nonlinear evolution of a vortex sheet with an initially sinusoidal vorticity distribution and subject to a uniform strain. The origin of the strain and the general geometry are similar to those in figure 15, but the longitudinal vortices are now long flat ribbons of weak diffuse vorticity. In their calculations, these ribbons first rotate along a longitudinal axis and then collapse into compact longitudinal cores, similar to the ones hypothesized above. The collapse time is proportional to T/S^2 and, for large S, is generally much shorter than the equilibration time of (1). Therefore, the model of a longitudinal vorticity distribution collapsing rapidly into an array of compact streamwise vortices which then deform the interface in a manner approximated by the model used in this section is not only suggested by the three-dimensional reconstruction but theoretically consistent.

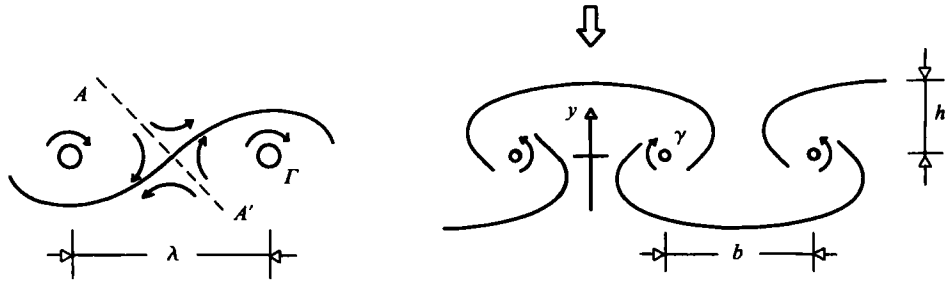

FIGURE 15. Deformation of the interface by the streamwise vortex system.

The time T is also the characteristic evolution time for the spanwise structures, so that (2) describes the deformation amplitude of the interface during most of its lifetime. Since everything in that equation, except for the circulation ratio, can be measured from the visualization pictures, the equation can be used to estimate the ratio γ/Γ.

We used the low Reynolds number film to measure as many structures as possible. The whole film was analysed, but only those braids that were not involved in amalgamations and only those structures whose vortex centres could be determined with some certainty were used. Out of 18 braids in the film, only 7 were considered useful, containing a total of 23 good pairs. Of these, 18 are contained in 4 braids, each containing 3 or more structures. These braids were used for the computation. Even so, the scatter of the data was large.

The streamwise distance between primary eddies was estimated from these measurements to be

$$\frac{\lambda}{x} = 0.694 \frac{U_1 - U_2}{U_1 + U_2},$$

which is large compared to other published values, but within the allowable range. This is probably not too significant since the mixing layer, at this station, is not yet in the self-similarity region. The ration between span and streamwise wavelengths is $2b/\lambda = 0.38 \pm 0.14$, in rough agreement with the value of 0.463 given in Jimenez (1983). Note that this is true even if the velocity ratios are very different, in agreement with the stability theory (Pierrehumbert & Widnall 1982) which predicts both wavelengths as fixed fractions of the layer thickness.

The angle formed by the longitudinal vortices with respect to the free stream is $48 \pm 10°$, consistent with the assumption that they lie on the 45° cat's-eye streamline. The planes that contain the longitudinal vortex pairs are almost parallel to the spanwise axes ($-2 \pm 20°$), although with a large scatter which probably reflects the fact that a row of alternating vortices is always linearly unstable. All these data are consistent with our simplified model; the measured value for the aspect ratio is $h/b = 0.58 \pm 0.22$, and the value computed for the circulation of the longitudinal vortices is $\gamma/\Gamma = 0.61 \pm 0.79$.

The scatter of these values is quite high but the vorticity estimate itself is probably fairly robust. The largest source of error in the simplified model is probably the assumption that the longitudinal vortices are located at their equilibrium positions. We have noted above that a row of alternating vortices is always unstable, and many structures in the film are in fact found to be tilted with respect to the span. A first approximation to the effect of these motions on the vorticity estimate can be

computed by assuming that only the two nearest cores are important for a given structure, and by linearizing the equation. The result of applying this correction to the braids used before, is a new estimate of $\gamma/\Gamma = 0.58 \pm 1.13$, which is consistent with the previous one.

The evidence in Jimenez (1983) suggested that the streamwise vortices have a more or less constant circulation so that the ratio γ/Γ decreases downstream. It is convenient, therefore, to give their circulation as a fraction of a constant quantity such as the circulation Γ_0 contained in each wavelength of the initial primary instability. The spanwise circulation at a given section is proportional to the primary wavelength, and the ratio Γ/Γ_0 can be estimated by the ratio λ/λ_0. The initial wavelength was not measured directly in this experiment but, using the momentum thickness given in table 1, and assuming that $\lambda = 35\theta$, we get a value of $\gamma/\Gamma_0 = 1.59 \pm 2.08$. A value between 1 and 1.5 was found in Jimenez (1983) for this parameter; it was obtained for a half-jet by a completely unrelated method involving the spanwise nonuniformity of longitudinal velocity.

6. Conclusions

We have presented three-dimensional reconstructions of the concentration field of a nominally plane mixing layer. In the downstream station corresponding to the developing region of the three-dimensional transition, the reconstruction shows longitudinal structures which are not only very marked, but strikingly well organized. Those structures give strong support to the interpretation that they are due to an array of longitudinal alternating vortices which form a system separate from the main spanwise eddies, in general agreement with the model in figure 1.

This is particularly true of the flow in the braids and above and below the vortex cores. On the other hand, the loops joining consecutive longitudinal vortices in figure 1 are conceptualizations based on the idea that vortex lines have to be continuous. In actual flows, especially at higher Reynolds numbers, the vortex lines from both systems are likely to be tangled in this region, making any discussion of individual vortices, on that part of the flow, basically meaningless.

At low Reynolds numbers, this zone of intersection of the two orthogonal vortex systems seems to control the location of small-scale mixing. Further downstream, the longitudinal structure persists but it is now submerged in a broader region of generalized mixing and its dynamical significance is harder to decide.

The strength of the longitudinal vortices is a large percentage of the local circulation in the spanwise eddies, and is roughly once or twice the initial circulation of the spanwise vortex system. This suggests that their origin is some three-dimensional instability of the spanwise structure, either before or after the first pairing interaction.

The research of one of the authors (L. P. B.) was partially supported by the Office of Naval Research, contracts numbers N00014-79-C-0365 and N00014-76-C-0260. M. Cogollos was partially supported by an IBM study fellowship. We want to acknowledge the help of Dr M. A. Hernan of the Jet Propulsion Laboratory in digitizing some of the film sequences used in this paper and in the measurements leading to the vortex pair strength. J. L. Navalon is responsible for much of the contour extraction software. Dr A. Roshko contributed with many helpful discussions in the interpretation of the pictures.

REFERENCES

BERNAL, L. P. 1981*a* The coherent structure in turbulent mixing layers. I. Similarity of the primary vortex structure. Ph.D. thesis, Caltech.

BERNAL L. P. 1981*b* The coherent structure in turbulent mixing layers. II. Secondary streamwise vortex structure. PhD. thesis, Caltech.

BREIDENTHAL, R. E. 1981 Structure in turbulent mixing layers and wakes using a chemical reaction. *J. Fluid Mech.* **116**, 1–24.

BROWAND, F. K. & TROUTT, T. R. 1980 A note on spanwise structure in the two-dimensional mixing layer. *J. Fluid Mech.* **97**, 771–781.

BROWN, G. L. & ROSHKO, A. 1974 On density effects and large structure in turbulent mixing layers. *J. Fluid Mech.* **64**, 775–816.

CORCOS, G. M. 1979 The mixing layer: deterministic models of a turbulent flow. *Rep.* FM-79-2 *Univ. California, Berkeley.*

DIMOTAKIS, P. E., MIAKE-LYE, R. C. & PAPANTONIU, D. A. 1983 Structure and dynamics of round turbulent jets. *Phys. Fluids* **26**, 3185–3192.

FOLEY, J. D. & VAN DAM, A. 1982 *Fundamentals of Interactive Computer Graphics.* Addison-Wesley.

HERNAN, M. A. & JIMENEZ, J. 1982 Computer analysis of a high-speed film of the plane turbulent mixing layer. *J. Fluid Mech.* **119**, 323–345.

HUSSAIN, A. K. M. F. & CLARK, A. R. 1981 On the coherent structure of the axisymmetric mixing layer: A flow-visualization study. *J. Fluid Mech.* **104**, 263–294.

JIMENEZ, J. 1983 A spanwise structure in the plane mixing layer. *J. Fluid Mech.* **132**, 319–336.

JIMENEZ, J. & NAVALON, J. L. 1982 Some experiments in image vectorisation. *IBM J. Res. and Development* **26**, 724–734.

KONRAD, J. H. 1976 An experimental investigation of mixing in two-dimensional turbulent shear flows with applications to diffusion-limited chemical reactions. Ph.D. Thesis, Caltech.

LIN, S. J. & CORCOS, G. M. 1984 The mixing layer: deterministic models of a turbulent flow, Part III: the effect of plane strain on the dynamics of streamwise vortices. *J. Fluid Mech.* **141**, 139–178.

PHONG, B. T. 1975 Illumination for computer generated pictures. *Comm. ACM* **18**, 311–317.

PIERREHUMBERT, R. T. & WIDNALL, S. E. 1982 The two- and three-dimensional instabilities of a spatially periodic shear layer. *J. Fluid Mech.* **114**, 59–82.

ROSHKO, A. 1980 The plane mixing layer, flow visualisation results and three-dimensional effects. In *The Role of Coherent Structures in Modelling Turbulence and Mixing* (ed. J. Jimenez). Lecture Notes in Physics, vol. 136, pp. 208–217, Springer.